Ice plate deformation and cracking revealed by an in-situ distributed acoustic sensing array

Jun Xie[1], Xiangfang Zeng[1], Chao Liang[2], Sidao Ni[1], Risheng Chu[1], Feng Bao[1], Rongbing Lin[1], Benxin Chi[1], Hao Lv[1]

[1] State Key Laboratory of Geodesy and Earth's Dynamics, Innovation Academy for Precision Measurement Science and Technology, Chinese Academy of Sciences, Wuhan, 430077, China
[2] Institute for Disaster Management and Reconstruction (IDMR), Sichuan University, Chengdu, 610100, China

Correspondence to: Xiangfang Zeng (zengxf@whigg.ac.cn)

Abstract. Studying~~The study of~~ seismic sources and wave propagation in ice plate ~~is helpful to understand~~can provide valuable insights into understanding various processes such as ~~the~~ ice structure dynamics, migration, fracture mechanics, mass balance and ~~other processes~~more. However,~~ due to~~ the extreme environment presents challenges that result in limited ~~,~~ in-situ dense seismic observations. Consequently, our understanding of the dynamic changes within the ice sheet remains insufficient. ~~are rare and the dynamic changes of the ice plate remain poorly understood.~~ We conducted a seismic experiment ~~with~~ using a distributed acoustic sensing array on a frozen lake,~~.~~ ~~We~~ exciting~~e~~ water vibrations through~~by~~ under~~-~~water airgun shots. By employing an~~With an~~ artificial intelligence method, we were able to detect~~ed~~ seismic signals that includes~~ing~~ both high frequency icequakes and low frequency events. The i~~I~~cequakes clustered along ice~~ the~~ fractures and correlated with~~ the~~ local temperature variations. The waveforms of Low frequency events exhibit characteristics of flexural-gravity waves which offer insights into~~. The flexural-gravity wave reveals~~ the properties~~y~~ of the ice plate. Our study demonstrates the ~~utility~~ effectiveness of a Distributed Acoustic Sensing~~DAS~~ array as an in-situ dense seismic network in ~~illuminating~~ for investigating the internal failure process and dynamic deformation of ice plate such as ice shelf. This research~~, which~~ contributes to an enhanced comprehension and ~~understanding~~ ~~and~~ prediction of ice shelf disintegrations~~ of ice shelves~~.

1 Introduction

Cryo-seismology, due to its~~ can provide~~ high temporal resolution ~~results~~ capabilities, has attracted the attention of scientists in the fields of seismology, ~~cryosphere~~cryosphere, and climatology. It serves as a valuable tool for investigating~~for the study of~~ glacier dynamics and comprehending intricate processes~~,~~ ~~thus attracting the attention of scientists from seismology, cryosphere and climatology~~ (Aster and Winberry, 2017; Podolskiy and Walter, 2016). Seismological records of the cryosphere can be ~~used~~ utilized to study the dynamic process ~~of~~ occurring on the surface or ~~interior~~ within ~~of the~~ glaciers, thereby facilitating the identification of~~so as to reveal~~ the ice shelf damage and~~,~~ environmental changes and other fields. Large glacial earthquakes can be ~~recorded~~ detected by ~~almost~~ global seismic networks (for example GSN), and their mechanisms ~~they~~ have been ~~well~~ extensively studied~~.~~, which are considered to be associated with ~~to inferring the process of~~

iceberg calving and capsizing (Ekström et al., 2003; Sergeant et al., 2019; Veitch and Nettles, 2017). However, local microseismicities (such as surface crevasses and basal slip eventsopening and development) can better revealprovide more insight into the dynamic change process of glaciers and be used tofacilitate the study of glacier disintegration the mechanism of glacier disintegration (Helmstetter et al., 2015; Lombardi et al., 2019; Romeyn et al., 2021; Walter et al., 2013). Due to low seismic energy and high attenuation associated with these events, it is crucial to have closely spaced seismic station we need close stations (e.g., on the ice surface or in shallow boreholes) in order to accurately capture and analyse the data (Röösli et al., 2014; West et al., 2010). However, the complex environment and heavy logistical challengess of glaciers make it difficult to install deploy in- situ seismometers for comprehensive monitoring. As a result, Some researchers even even studied explored the potential of using utilizing aone single seismometer to study icequakes (Köhler et al., 2019).

In recent years, the use of distributed acoustic sensing (DAS) arrays has been tested in glacier environments to study glacial structures and with advantage of large aperture and dense observation has been tested on glacier environment to study the glacial structure and detect its seismicities (Booth et al., 2020; Brisbourne et al., 2021; Castongia et al., 2017; Fichtner et al., 2022; Hudson et al., 2021; Walter et al., 2020). Hudson et al. (2021) explored conducted a study on using DAS to monitor basal icequakes at Rutford Ice Stream. In their research, tThey compared the performance of DAS with a geophone network in terms of for microseism detection and location. The studyAnd found the DAS is superior outperformed the geophone network infor recording monitoring the microseism signals. Their methodology and implications findings are heuristic for the applying of DAS in glacial environment. Walter et al. (2020) deployed a DAS network in Alpine terrain and they successfully detected glacier stick-slip events which are associated related with glacier flow and nearby rock falls. Their work demonstrated the significant potential of DAS technology for seismic monitoring of glacier dynamics and natural hazards in the mountain region. These work studies demonstrated logistical feasibility of installing a large, high-quality DAS network in a glacial environments. However, the deployment of DAS on ice shelves for studying the interaction between water and ice has been limited.

In this study, we deploy a DAS network on the Xiliushui Reservoir, a frozen lake, the Xiliushui Reservoir in Gansu Province, China to investigate explore the utility effectiveness of using of a DAS array in for monitoring the cracking and dynamic flexure of the ice plate (Fig. 1). Seismicitiesy haves been observed on frozen lakes similar to icequakes in ice shelf (Dobretsov et al., 2013; Kavanaugh et al., 2018; Ruzhich et al., 2009). Nziengui-Bâ et al. (2022) measured the thickness and Young's modulus of the ice pack of a lake with DAS using hammer signal. Fichtner et al. (2022) deployed fiber-optic cableoptical fiber on a frozen lake of a volcano and . They detected the volcanic tremor. In our study, wWe excite employed water waves using an underwater AirGun Excitation (AGE) to generate water waves and, and recorded the resulting water vibrations of water. Using an AI- based method, we successively detected and classifiedy various the abundant seismic events, including both icequakes and Low Frequency Events (LFEs). Subsequently, wWe then conducted an analysis of the seismic signals, examining their waveformze the characteristics, occurrence rates and locations. One of the key aspects of our analysis involved estimating the and physical mechanism of the seismic signals through the waveform, occurrence rate and location. The stiffness of the ice plate is by studying estimated with the dispersion of the flexural-gravity waves excited by LFEs. Finally, we discussed implications of our experiments for studying understanding theice shelf dynamics of ice shelves in natural settinge.s.

设置了格式: 字体: (中文) +中文正文 (宋体), (中文) 简体中文(中国大陆)

2 Experimental setting

The experimental site for our study wasis at the Zhangye airgun active source platform, which locatedis in Xiliushui Reservoir, the secondary reservoir of Zhangye Longshou Hydropower Station in Qilian Mountain, Zhangye City, Gansu Province, China (Fig. 1). The average elevation of the Zhangye airgun active source platform is approximately ~1900 meters. The water depth of the lake Xiliushui Reservoir ranges fromis 45 to -65 meters, and during the winter of Northern Hemisphere, the ice thickness in the reservoir reaches aroundis ~0.5 meters in North Hemisphere winter. The active airgun source used in this study wasis positioned located atin the centre of the lake, submerged at a depth of 15 meters beneath low the water surface (Wei et al., 2018). It has been observed that the bBubbles generated -excited by the airgun can produce induce water vibrations, as described in the study by (de Graaf et al., (2014). This makes the airgun an effective, which is a good active source source for simulating ocean waves. The generated water vibrations closely resemble the characteristics of natural ocean waves, allowing for realistic and controlled experiments in the study of ice and wave interaction and related phenomena.

In our experiment, aA 1.2 km long fiber-optical cable was deployed installed on the surface of the ice from during the period of January 6th to January 9th, 2020. The fiber-optical cable was laid in two circular patterns around the airgun floating platform in two circles. The inner circle is about about 340 meters long, spanning -(channels 470 to -645), and the outer circle is nearly 800 meters long, encompassing (channels 51-457) (Fig. 1). To ensure proper coupling between the fiber-optic cable and the ice surface, wWe poured the optical cablewater over the fiber-optic cable with water.. Aas the water froze, it formed a solid bond with the ice, effectively coupling the fiber-optic cable to the ice surface. the optical cable was well coupled with the ice surface. The interrogator is Silixa iDASan Ovlink DAS unit and the cable is a standard single-mode fiber-optic cable. In this experiment, we employed athe gauge length ofis 210 meters, which refers to the length of the section of the fiber-optic cable used for measurements.. Tthe spatial sampling interval wasis set at 2 meters, and the temporal sampling rate was set atis 1000 Hz. The experiment started commenced at 21:00 p.m. on January 6th (Beijing time) and ended concluded at 17:00 p.m. on January 9th. Unfortunately, sSome instrument failures occurred in during the afternoon of January 8th, resulting in an inand there was no complete record from between 11:00 p.m. to and 13:00 p.m. During the entire duration of the experiment, aA total of 65 hours of data, amounting to nearly 600 GBTB of data was recorded. In Aadditionally, there was a CMG-40T three-component short-period seismometer, equipped with a RefTek 130B data logger, was positioned on the shore to record capture ground motion. This seismometer recorded data at , with a sampling rate of 50 Hz, providing complementary information to the recordings obtained from the fiber-optic cable setup on the ice surface.

3 Seismic events

ThroughoutDuring the experiment, a total of 239 AGEs were carried conductedout in total. However, dDue to anthe instrumental issue, only 223 complete AGEs were successively recorded. Previous studies found indicated that the near-field AGE waveform mainly consists comprises of two partscomponents:, the main pulse and low-frequency bubble signal 2. However, our observations with DAS revealed we found that the near-field AGE signal recorded by DAS has exhibit a distinctno main pulse (Fig. S1 in the supporting information)., and Additionally, we observed that the similarity of between different AGE waveforms was less below than 20% (Fig. S2 in the supporting information). The main reason for this phenomenon may is likely be to related tothat the short observation distance – between the DAS array and the airgun source.was too short, This proximity may have causedand the signal recorded by DAS record was to be clipped, resulting in the absence of a recognizable main pulse.

In addition to the AGE experiments, wWe also conducted ten hammering experiments to measure the velocity of seismic waves propagating in the ice. The main energy of hammering signal primarily contained energyis above 100 Hz (Fig. S1 in the supporting information). In the hammering signal, aA relatively weak P wave signal can be seen in the DAS record on the ice surfacobservede. By analysingUsing the DAS record alongin a line aligned with the hammering point, we estimated that the P wave velocity in the ice to be approximatelyis ~3,200 m/s (Fig. S3 in the supporting information)., This estimation is consistent with previous research findings. For instance, studyies conducted by (Ewing et al., (1932004) have indicated that thick solid ice typically exhibits P-wave velocitiyes ranging between 3,432 and 3,698 m/s. Similarly, (Wen et al., (1991) reported that thinner ice layers are expected to have velocities ranging from 2,000 to 3,040 m/s.which is consistent with previous studies (e.g., Castongia et al., 2017).

Besides Apart from the AGE and hammering signals, ourwe observations revealeded two types of passive source signals (Fig. 2). The first typekind corresponds to is icequakes that occur within the ice plate and are characterized by a within the ice plate dominantted by energy at high frequenciesy ranging (from over >10 Hz to a few hundreds of Hz (Fig. 2). These signals are associated with longitudinal waves propagating through the ice plate that cause the elongation along the fibre directionThey correspond to longitudinal waves in the and the elongation associated with flexural waves which propagate along the fiber direction ((Moreau et al., , 2020). During the occurrence ofWhen some icequakes occurred, the staff also reported hearingheard the cracking sounds, which aligns , consistent with previous observations reported by (Kavanaugh et al., (2018). This acoustic evidence provides further confirmation of the dynamic activity within the ice plate during seismic events. The other type is characterized by energy primarily in the lower frequency range (1-10 Hz) and has a duration of approximately 1 second (Fig. 2)kind., We termed them as Low Frequency Event (LFE). (Fig. 2), is dominated by energy in the lower frequency band (1-10 Hz) and has a duration of nearly 1 s. TheThese LFEsy typically , emergeding primarily after AGEs and exhibit remarkably , share very similar waveforms and moveouts as depicted in (Fig. S4 in the supporting information).

4 ~~Seismic events~~ D~~d~~etection and location

The application of machine learning in seismology has experienced a significant growth in recent years. Machine learning techniques have been primarily focused on earthquake detection and phase-picking methods, often applied to regional and global earthquake that rely on conventional seismic networks (Zhu and Beroza, 2019; Zhou et al., 2019; Stork et al., 2020; Ross et al., 2018). In this study, we applied a convolutional neural network (CNN) known as You Only See Once (YOLO, version 5) (Redmon and Farhadi, 2018) to scan efficiently through the DAS data to detect the seismic events and classify them into three categories: AGE LFE and icequake. ~~(see Appendix A).~~ This CNN is designed for accurate real-time object detection in video files (Redmon and Farhadi, 2018) and has been successfully utilized for micro-seismic event detection in DAS records (Stork et al., 2020). W~~We~~e converted the record section of DAS waveforms to images. ~~to detect the seismic events and classify them into three categories: AGE LFE and icequake. YOLO was developed for accurate real-time object detection for video files~~ (Redmon and Farhadi, 2018)~~, which also has been used to detect micro-seismic event for DAS record (Stork et al., 2020).~~ To enhance the signal-noise-ratio (~~-~~SNR), the DAS data is bandpass filtered within the range of~~to~~ 5-50 Hz and normalized based on~~with respect to~~ the maximum amplitude of the entire record section. We assemble 6-second of data from ~~of~~ all channels (51-645) into an image, ensuring a~~with~~ 50% overlap to prevent misdetection. We then down~~-~~sample the image to a size of 600 by 600 pixels, resulting in ~~and keep~~ each image ~~size~~being approximately ~~to about~~ 980 KB in size.

To train the AI model, we manually inspected the seismic data ~~of~~ from the first 12 hours and labelled 60 AGEs,122 LFEs and 360 icequakes. This dataset was then divided this into training, validation, and test sets using a 4:1:1 ratio. The catalogue of AGEs was well-established and used to evaluate the performance of the model. To accelerate the training process, we utilized GPU, which reduced the training time to approximately 3 hours. The performance of the model on the test set is depicted in Fig. S5~~12~~. The confusion rate was found to be low, indicating accurate classification results. For instance, no AGEs were misclassified as icequake. The recall rate~~s~~ is the number of True Detectives (TP) divided by everything predicted as positive. TP is the True Prediction, that is, for example the icequake being detected as icequake. The recall rates for AGEs, LFEs and icequakes are 100.0%, 100.0% and 91.0%, respectively, while the ~~accuracy rates~~precision for the three are 73.0%, 93.0% and 62.8%.

~~The accuracy of AGE detection was affected by the strong amplitude of AGE signals, leading to misclassification of subsequent waveforms as AGEs by the model. However, the likelihood of such detections was very low. By adjusting the confidence score threshold to 0.7, the accuracy of AGE detection improved to 100%. This is evident because higher confidence scores correspond to higher accuracy, and this principle holds true for icequake detection as well. However, the accuracy of icequake detection is relatively lower compared to low-frequency and AGEs, which is understandable given the complex features exhibited by icequakes. Increasing the size of the training dataset should improve the accuracy of icequake detection. The limited availability of datasets poses a common challenge in DAS microseismic detection (Lv et al., 2022). This is evident because higher confidence scores correspond to higher accuracy, and this principle holds true for icequake~~

detection as well. However, the accuracy of icequake detection is relatively lower compared to low-frequency and AGEs, which is understandable given the complex features exhibited by icequakes. Increasing the size of the training dataset should improve the accuracy of icequake detection. The limited availability of datasets poses a common challenge in DAS microseismic detection (Lv et al., 2022). As research in the field of seismology with DAS continues to advance and more datasets become accessible, we can anticipate significant improvements in the accuracy of icequake detection. In our study, we not only evaluated the model's performance using the test dataset but also tested it on data that were not included in the test dataset. We found that the accuracy of icequake detection was already relatively high, reaching 85%. This level of accuracyprecision is comparable to the results reported by Stork et al. (2020), indicating statistically meaningful characteristics of the study area.As research in the field of seismology with DAS continues to advance and more datasets become accessible, we can anticipate significant improvements in the accuracy of icequake detection. In our study, we not only evaluated the model's performance using the test dataset but also tested it on data that were not included in the test dataset. We found that the accuracy of icequake detection was already relatively high, reaching 85%. This level of accuracy is comparable to the results reported by Stork et al. (2020), indicating statistically meaningful characteristics of the study area. Finally, we apply trained AI model to scan through the rest of the seismic data (39,280 images). In total, we detected 14,498 icequakes and 9,391 LFEs.

Using an AI based method You Only See Once (YOLO) (Redmon and Farhadi, 2018), we scan efficiently through the DAS data (see Appendix A). The AGE catalogue indicates the accuracy of the detection method. To gain deeper insights into thefurther determine the mechanism of the seismic sources, we locate the detected identified icequakes and LFEs, respectively (see Appendix B). Here, we utilize an absolute location method based on the neighbourhood algorithm (Sambridge, 1999) for precise determination of the seismic source locations. We locate the seismic events using an absolute location method based on the neighbourhood algorithm (Sambridge, 1999) with the first arrivals. We assume that the propagation velocity of seismic waves in the ice sheet is isotropic,We assumed a constant seismic velocity in all directions, since the structure of the site is relatively simple, and set it as an inversion parameter. Since the ice plate is thin, we assume the focal depth to be zero. We used a STA/LTA method (Stevenson, 1976) to pick arrivals. The short and long time-windows are set to 0.05 s and 0.25 s for icequakes, and 0.5 s and 2.5 s for LFEs, respectively. The travel time misfit is normalized by the maximum amplitude of each waveform, taking into account amplitude information. To assess the location error of our location method, we located those 10 hammering events. The results showed that the minimum, maximum and average location errors of hammering events are 5 m, 20 mm, and 10.2 m, respectively (Fig. S613 in the supporting information). It is important to note that most of the location results exhibited a bias towards the north direction. This systematic deviation of the location results could be attributed to the systematic bias in the position of fiber-optical cable. fiberOverall, the number and accuracy of arrival picks can also influence the location accuracy, the accuracy of the location in this study is acceptable. It is important to carefully assess and address factors such as the cable position bias and the accuracy of arrival picks. By minimizing these sources of error and improving the data quality, the accuracy of event location estimation can be enhanced in DAS-based seismic monitoring applications.

We detected 14,498 icequakes, exhibiting a clear diurnal cycle (Fig. 2c) and primarily clustered along the promising fractures (Fig. 2d). The number of icequakes does not seem to be associated with AGEs but is rather correlated with the local temperature variation (Fig. 2c). This phenomenon has also been reported by other studies, for instance, (Goto et al., (1980) observed that there was a strong correlation between the occurrence of high icequake activity and the temporal variation of temperature differences within the ice plate., consistent with other studies (e.g., Kavanaugh et al., 2018). Thisthese observations reveals the nature of icequakes in our experiments as brittle failure of ice plate caused by uneven thermal expansion. The icequake interevent distribution follows a Poisson distribution (Fig. S75 in the supporting information), indicating suggesting that the occurrence of icequakes is randomits randomness, similar to tectonic earthquakes (Rydelek and Sacks, 1989). This implies that there is no specific temporal or spatial pattern governing the occurrence of icequakes, and they occur independently of each other. It provides valuable insights into the nature of icequake occurrence . It indicates that icequakes, like tectonic earthquakes, can be considered as stochastic processes, and their occurrence is not predictable based on a regular or periodic pattern.in the ice plate. This information is important for understanding the behaviour of icequakes and their relationship to other geophysical phenomena. These observations reveal the nature of icequakes in our experiments as brittle failure of ice plate caused by uneven thermal expansion. It is worth notingThus, the surge of icequake activity since the noon of January 9th probably indicates a heightened development of cracks within the ice plate. There also seems to be a slight delay between the icequake activity and the temperature, which is probably due to lag from thermal diffusion. According to the study of (Goto et al., 1980), the time lag is about 2 hours. In our study, we did not directly measure the ice temperature, but instead relied on the air temperature data. Future work should consider incorporating a combined approach using distributed temperate sensing (DTS) (Selker et al., 2006) as well as in-situ DAS observations to establish a more accurate correlation between temperature variations and seismic activity. –Besides, to gain a more comprehensive understanding of the relationship requires a longer observation period in real glacial environments.However, a robust establishment on the relationship requires a longer observation.

Out of the total number of detected events, 9,391 LFEs were observed.A total of 9,391 LFEs are detected, mostly clustered in the centre of the lake, and close to the airgun floating platform These LFEs exhibit a tendency to cluster primarily in the central region of the lake, as well as in close proximity to the airgun floating platform (Fig. 2d). The analysis reveals a close association between LFEs and AGEs, with LFEs generally following AGEs closely in time. However, the detectability of LFEs may vary for different AGEs due to varying noise levels. It is observed that LFEs become more challenging to observe approximately 5 minutes after the occurrence of AGEs (Fig.ure 2c and further supported by Fig.ure S8 in the supporting information). LFEs tend to follow the AGEs tightly (although vary in detectable numbers for different AGEs depending on noise levels), and are difficult to observe 5 minutes after AGEs (Fig 2c and Fig. S6 in the supporting information). In the meantime, tThe interevent occurrence of LFEs does not follow a Poisson distribution (Fig. S97 in the supporting information). ,These observations suggest that there may be a temporal relationship or dependency between

AGEs and LFEs, indicating potential interactions or triggering mechanisms between these seismic events and LFEs are likely~~ indicating that they are not random events but likely triggered by~~ the water vibrations following the AGEs~~ that has been widely observed~~.

5 Dispersion curve of LFE

Extracting the dispersion relation from the waveforms of LFEs is a valuable approach to gain a deeper understanding of their physical mechanism and signal propagation.~~To gain a deeper understanding of the physical mechanism of LFEs and its signal propagation, we extract the dispersion relation from the waveforms of LFEs.~~ In order to enhance the signal-to-noise ratio (SNR) of the LFEs, we employed a technique of waveform stacking. This is applicable because the LFEs waveforms share a similar moveout patterns (Fig.~~ure~~ S4 in the supporting information). By selecting a master LFE event, we aligned the waveforms of other LFEs by measuring the time shifts through cross-correlation analysis. This stacking process involves adding up the aligned waveforms, which effectively increases the amplitude of the coherent LFE signals while reducing the contribution of random noise. As a result, the stacked waveform provides a clearer and more distinct representation of the LFE activity, allowing for better analysis and interpretation of the underlying physical mechanisms. ~~Since the LFEs share rather similar waveforms and moveout pattern (Fig. S4 in the supporting information), we take a master LFE event and stack the waveforms of other LFEs with time shift measured via cross correlating to enhance the signal-to-noise ratio (SNR).~~ As a quality control, we applied a threshold for the cross-correlation coefficient to retain only the waveforms that exhibited a strong correlation with the master LFE event. Specifically, we considered waveforms with a cross-correlation coefficient greater than 0.7 as indicative of a significant correlation. This criterion ensured that only high-quality waveforms were included in the stacking process.~~we only retain waveforms with cross-correlation coefficient greater than 0.7 and the resulting stacked waveforms are shown in Fig. 3 with a clear inverse dispersion.~~ The resulting stacked waveforms, which are shown in Fig.~~ure~~ 3, exhibit a clear inverse dispersion pattern. This pattern implies that the LFEs with higher frequencies arrive earlier than those with lower frequencies.

After obtaining the stacked LFE waveforms, we applied the multi-channel surface wave analysis method developed by ~~(~~Park et al.~~,~~ (1999) to extract the phase velocity dispersion curve. This method allows us to analyse the surface wave signals present in the stacked LFE waveforms and determine the variation of phase velocity with respect to frequency.~~We then apply the multi-channel surface wave analysis method (Park et al., 1999) on the stacked LFE waveforms and extract the phase velocity dispersion curve.~~ In the frequency range of 1 to 15 Hz, the phase velocity of the LFEs varies from 20 to 160 m/s. This range of velocities is significantly lower than the typical shear wave velocity of ice, which is around 1400 m/s as reported by ~~(~~Hudson et al. ~~,~~ (2021). ~~The phase velocity increases with frequency and varies from 20 to 160 m/s in 1 to 15 Hz (Fig. 3c), much lower than the typical shear wave velocity of the ice (~1400 m/s, Hudson et al., 2021).~~ This dispersion curve displays the distinctive characteristic of the ~~has the canonical trait~~Flexural-Gravity Wave (FGW) (Williams and Robinson, 1981), which ~~of~~is a special guided wave driven by restoring forces from~~that occurs~~ ~~along a suspending ice shelf~~

as a result ofdriven by the interplay between of ice plate flexure and gravity., namely the Flexural-Gravity Wave (FGW) (Williams and Robinson, 1981) whichIt corresponds to the quasi-Scholte mode (QS) seismic wavefield of a floating ice plate (Moreau et al., 2020; Nziengui-Bâ et al., 2022).

The dispersion relation (relation of frequency (f) and wavenumber (k)) forof FGW can be written as (Liu and Mollo-Christensen, 1988),

$$(2\pi f)^2 = \frac{(gk+Dk^5-Qk^3)}{\coth kH+kM} \quad (1).$$

g is gravity, k is wavenumber, H is the water depth which is 60 meters in this study. D is the bending modulus, which is a function of ice properties, $D = Eh^3/\rho_w 12(1-v^2)$, where E is the Young's modulus, υ is the Poisson ratio, h is the ice thickness which is 0.5 meters in this study, ρ_w is the density of water. Q is due to compression forces, $Q = Ph/\rho_i$, where ρ_i is the density of ice. M is due to the added mass of the ice sheet, $M = h\rho_i/\rho_w$. Q and M areis much smaller than gravity and flexural terms and can be neglected (Sutherland and Rabault, 2016). The dispersion equation can be rewritten as,

$$(2\pi f)^2 = \frac{(gk+k^5Eh^3/\rho_w 12(1-v^2))}{\coth kH+kM} \quad (2).$$

The Young's Modulus can also be determined with compressional wave velocity Vp, $E = V_P^2\rho(1-v^2)$, assuming v=0.33, according to the results from Fig. S3, E is 9.12 GPa.

The dispersion of the FGW is largely controlled by the ice plate thickness and stiffness (Zhao et al., 2018; Sergienko, 2017; Sutherland & Rabault, 2016; Timco & Frederking, 1983; Yang & Yates, 1995). Given a roughly known ice plate thickness (~0.5 m), we successfully explain the observed dispersion curve using the theoretical prediction of FGW (equation 1 in reference Sutherland & Rabault, 2016, and Appendix C) with an ice Young's modulus (E) around 10 GPa. Following a Bayesian scheme, both thickness and the Young's modulus can be estimated (Nziengui-Bâ et al., 2022). In this case, the Young's modulus is 9.41±0.12 GPa, and the thickness is 48±0.1 cm, respectively.a.

Indeed, tThe effective modulus of ice is a measure of itscan be regarded as an indicator of the elastic and viscous deformation characteristics, which can be influenced by various factors, includingthat is dependent on the strain rate, temperature, density, ice type and, purity etc. (Sinha, 1989). Considering the complex nature of ice and its sensitivity to various factors, understanding the effective modulus provides valuable insights into the deformation behaviour and mechanical properties of ice under different conditions. Researchers study these relationships to improve our understanding of ice mechanics and its applications in various fields, such as glaciology, geophysics, and engineering. And the Young's Modulus for different types of ice is very similar at a constant temperature. In the study of Nziengui-Bâ et al. (2022), the Young's Modulus are below 5 GPa. They suspected that the value of E is underestimated due to snow layer covering the ice surface or inhomogeneity/porosity of the solid columnar ice layer. In this study, the lake surface is covered with clear ice free from snow, implying a stronger stiffness., (Gold, 1988)(Northwood, 1947)(Petrovic, 2003)which is consistent with previous researches (Gold, 1988; Northwood, 1947; Petrovic, 2003). In the study by Gold (1988), the Young's modulus of the ice plate was found to be within the range of 4.7-10.4 GPa. This range represents the stiffness or rigidity of the ice material, with higher values indicating greater stiffness. Northwood (1947) conducted an inversion analysis and estimated the Young's modulus of ice to be 9.8 GPa. This value falls within the range reported by Gold (1988) and provides additional support for the stiffness of ice. Another study by Petrovic (2003) reported a slightly wider range for the Young's modulus of ice, between 9.7 and 11.2 GPa. This range encompasses the values reported by both Gold (1988) and Northwood (1947), indicating consistency in the estimation of ice stiffness.

6 Discussion

Indeed, the effective modulus of ice is a measure of its elastic and viscous deformation characteristics, which can be influenced by various factors, including strain rate, temperature, density, ice type, purity and existence of cracks etc. (Sinha, 1989). Considering the complex nature of ice and its sensitivity to various factors, understanding the effective modulus provides valuable insights into the deformation behaviour and mechanical properties of ice under different conditions. Researchers study these relationships to improve our understanding of ice mechanics and its applications in various fields, such as glaciology, geophysics, and engineering. In the study of Nziengui-Bâ et al. (2022), the Young’s Modulus are below 5 GPa. They suspected that the value of E is underestimated due to snow layer covering the ice surface or inhomogeneity/porosity of the solid columnar ice layer. In this study, the lake surface is covered with clear ice free from snow, implying a stronger stiffness. In the study by Gold (1988), the Young's modulus of the ice plate was found to be within the range of 4.7-10.4 GPa. This range represents the stiffness or rigidity of the ice material, with higher values indicating greater stiffness. Northwood (1947) conducted an inversion analysis and estimated the Young's modulus of ice to be 9.8 GPa. This value falls within the range reported by Gold (1988) and provides additional support for the stiffness of ice. Another study by Petrovic (2003) reported a slightly wider range for the Young's modulus of ice, between 9.7 and 11.2 GPa. This range encompasses the values reported by both Gold (1988) and Northwood (1947), indicating consistency in the estimation of ice stiffness.

In this study, the seismic events are detected and located with using a dense DAS array, which has demonstrates a promising capability for high detection abilityrates. Further development is needed for machine learning-based techniques in extracting seismic phase arrival times from DAS seismic records in order to adapt to different DAS application scenarios. PhaseNet (Zhu and Beroza, 2019) is a relatively mature and reliable deep-neural-network-based method for phase extraction. As a comparison, Wwe detect seismic events using one reference seismometer onshore with another deep-neural-network-based seismic arrival picking method (PhaseNet) (Zhu and Beroza, 2019). A total of 2,348 events are have been detected in this study (Fig. S108 in the supporting information), and they exhibit good agreement all of them agreed well with the icequakes detected on DAS record by YOLO, albeit a lower but about count (approximately 6 times fewer). When aApplying PhaseNet toon a single channel of DAS (channel 150), a higher number of does result in more detected events are detectedthan the compared to the record from the onshore seismometer record (Fig. S108 in the supporting information).

However, this but also comes with a higher rate of false detection srate, probably likely because PhaseNet was not trained specifically with icequake data. MoreoverFurthermore, uponthrough visual inspection, we havealso confirmed that none of the LFEs were detected by PhaseNet. This outcome is not surprising sinceunexpected as PhaseNet was trained usingwith tectonic earthquake data, which shares more similaritiesy with icequakes than LFEs. In the future, incorporating DAS records in may be added to the training set of PhaseNet may enhance itsand improve the performance in detecting and picking the arrival time of icequakes and LFEs. The delay of the icequakes occurrence and the temperature may be probably due to lag from thermal diffusion. We did not directly measure the ice temperature but used the temperature data of the air. Future work warrants a combined distributed temperate sensing (DTS) (Selker et al., 2006) and DAS in-situ observation to provide a more accurate connection between temperature and seismic activity. Besides, a more complex distribution of the optic fibre, for example, the Zig-Zag array used in the PoroTomo project (Parker et al., 2018), can improve seismic event detection and location.

Deformations caused by induced by ocean waves, such as (e.g., FGW, play) have a significant role in the stability ofimpact on ice shelvesf and can potentially result in theirstability and may even lead to its fragmentation or trigger calving events (Collins III et al., 2015; Liu and Mollo-Christensen, 1988), however, previous studies have had limited direct observations of the dispersion of the FGW dispersion remained limited in previous studies (Sutherland and Rabault, 2016). In a study conducted by Fichtner et al. (2022), therecorded FGW was recorded usingwith DAS on the ice cap of a volcano., Tthey interpreted these recordings explained it as low-frequency volcanic tremor. In this work, we successfully obtained clear recordings of the FGW using DAS. By utilizing record of clear FGW and estimtheate known ice plate thickness, we can estimate the ice stiffness as the plate thickness is known. It is worth noting that iIn practical applicationse, the both thickness and stiffness can be estimated simultaneously under using a Bayesian scheme (Nziengui-Bâ et al., 2022).Actually,, the dispersion of FGW is more sensitive to the ice plate thickness, tThis approach holds significant value, particularly in cases where which is very valuable on ice shelf where the determination of ice thickness is not well resolved, as commonly encountered on ice shelves. Therefore, the accurate recording of FGW on DAS would be usefulprovides a valuable means for inferring both the ice shelf thickness and ice stiffness. For aIn the case of a cracked ice plate, it is commonly observed that the stiffness usually decreases, compared to the elastic modulus of the individual grains, which typically measures around (12 GPa). This suggest that, implying the thickness of the grain boundaries can could potentially bebe probably estimated with using the effective value of the modulus value (Wang et al., 2008). In our study, the presence ofDue to the AGE resulted in severe fracturing of, the ice plate close tonear the AirGun floating platform was severely fractured (Fig. 1). This localized fracturing indicateswhich implies that the Young's Modulus in this area may be smaller than compared that ofto the other placesregions. We measured the dispersion curves of FGW for inner circle and outer circle of the optical cable DAS records. The dispersion curves of FGW for inner circle results support corroborate our initial speculation (Fig. S1109 in the supporting information), which also provide an explainexplanation for the observed low phase velocity of FGW around 10 Hz in Fig. 3c. The dispersion curve of FGW measured obtained fromwit theh hammer signal (red triangle in Fig. 1) also revealsindicates a smaller Young's modulusE (Fig. S1210 in the supporting information). Specifically, in the inner circle, tThe Young's modulusE is estimatedclose to be approximately 7.5 GPa in the inner circle, which canis probably be attributeddue to the presence of intense fractures in that region. While oOur experiment was conducted over is limited to a 3-day period on a frozen lake spanningof a few hundred of meters, we acknowledge its limitations in terms of duration and spatial coverage. However, with longer continuous observation periods of LFEs, it becomesis possible to monitor the temporal change variations in stiffness or thickness of the ice shelf plate with longer continuous observation time of the LFE. By extending the observation time, we can gain valuable insights into the dynamic behaviour of the ice shelf and its response to environmental factors. Additionally, deploying a longer DAS cable holds the potential One may also expect to capture the attenuation effect of the ice plate, as highlighted by previous studies (Yang and Yates, 1995) effect upon deploying a longer DAS cable. -This would not only enhance our understanding of wave propagation characteristics but also provide valuable insights into the dynamic changes occurring within the ice plate and its response to environmental factors.

Previous studies have shown that FGW can has the potential to induce trigger icequakes on the ice shelvesf. The interaction between ocean waves and the ice shelf can lead to dynamic stress and strain variations, which can trigger seismic activities such as icequakes. For example,Studies such as Zhao -et al. (2019) have shown thatfound seismicity of icequakes exhibits spatial and seasonal associations correlations with ocean gravity waves. This association between icequakes and ocean waves suggests that the interaction between the two can have significant implications for the stability and integrity, ofthus affecting the integrity of the ice shelvesf and increasing the risk of ice shelf disintegration (Zhao et al., 2019). The energy transferred from the ocean waves to the ice shelf through processes like flexure and wave-induced vibrations can contribute to the fracturing and weakening of the ice, ultimately increasing the risk of ice shelf disintegration. (Olinger et al., (2019). Olinger et al. (2019) found thermal and tidal stresses are important in generating icequakes on the shelf., (Olinger et al., 2019). During In our experiment, we observed that the number of icequakes after the AGE did not show a change significant change after the AGE ly (Fig. S1231 in the supporting information). This suggests that there may not be a strong correlation, indicating the between the airgun shot or the FGW are probably not strongly correlated withand the occurrence of icequakes. It is important to note that the absence of a clear correlation in our experiment does not necessarily rule out the possibility of interactions between icequakes and these external factors in other contexts or under different conditions. We even observed a slight decrease in tThehe number of icequakes even decreases slightly after the AGE, which may duecould be attributed to the reduced detection capability reduced caused by strong AGE coda. This discrepancy highlights the potential may reflect structural difference between the ice plate on a frozen lake and a real ice shelf.; It emphasizes the importance of conducting more on-site seismic observations on real ice shelves to gain a deeper understanding of their dynamics and behaviour. Future studies incorporating comprehensive field observations on actual ice shelves will provide valuable insights into the seismic response and behaviour of icequakes, leading to a better understanding of the factors influencing their occurrence and the potential impacts on ice shelf stability. Moreover, DAS array on the seafloor is necessary to monitor the ocean wave and study the response of the ice shelf to the ocean waves Moreover, DAS array on the seafloor is necessary to monitor the ocean wave and study the response of the ice shelf to the ocean waves (Lindsey et al., 2019). which needs to be addressed by more on-site future seismic observations on real ice shelf.

Our work research highlightsshows that the considerable potential of DAS has important application potential toin monitoring the formation and development progression of ice cracks using passive source signals recorded in similar ice shelf studies, especially particularly in cases wherern there is a firn layer on the ice and optical methods such as remote sensing methods, it is difficult to use optical methodsare challenging to employ. In additionFurthermore, the variations of FGW can provide offer valuable information of about the inhomogeneity of ice plate stiffness inhomogeneity, which can probably potentially help infer the size and distribution of the ice plate fragments. It is important to note that oOur experiment wasis carried ouconductedt on the surface of an ice-covered lake, and to extend the applicability of these findings to to make it available on ice shelvesf, we need first to consider the spatial sampling to and optimization ofe the array layout should be essential considered. For example, by deploying fiber-optic cable spanning hundreds of meters, we of optical fibre can be used toaccurately locate ice-quakes with a precision of meter-level accuracys, and we can also measure FGW with a wavelength of dozens of meters. However, when it comes to For an ice shelvesf with a thickness reachingof hundreds of meters and a length spanningof tens of kilometres, to measuringe the FGW induced caused by ocean waves presents unique challenges. In these cases, (the corresponding the wavelength of FGW can extend tois several kilometres forat periods longer than 10 seconds ,(Zhao et al., 2018)., By extending the length of the fiber-optic cable to the spatial span of optical fibre should be several kilometres, we can probably capture FGW with larger wavelengths. However, tThere are other limitations that need to be addressed in the future studies, for example, the coupling of fiber-optic cables with the ice on real ice shelves presents a significant challenge in practical applications due to harsh environmental conditions. Moreover,. tThe conventional DAS fibre only measures a single strain component along the cable and does not provide polarization information, which increases the difficulty of identifying seismic phases (Hudson et al., 2021), and the absence lack of horizontal shear mode enlarges introduces additionalthe uncertainty in estimatingof ice properties estimation (Nziengui-Bâ et al., 2022). One potential remedy to address this is to use helically wound fibre but challenging for data processing (Ning and Sava, 2018). Moreover, DAS array on the seafloor is necessary to monitor the ocean wave and study the response of the ice shelf to the ocean waves (Lindsey et al., 2019).

7 Conclusion

In this study work, we deployed a dense DAS network on a frozen lake, allowing us to and captured a wealth ofbundant near-field seismic signals generated by various phenomena occurring within the ice plate. Specifically, we focused on two types of seismic events:produced by cracking, known as (icequakes) and dynamic flexure, referred as (LFEs) of the ice plate. We were able to obtain detailed and comprehensive recordings of these seismic signals. The icequakes, which are associated with cracking and fracturing of the ice, were detected, and analysed to understand their characteristics and spatial distribution. Additionally,accompanied by audible cracking sounds, clearly delineates the fractures on the ice plate. tThe LFEs, which result from the dynamic flexure of the ice plate, correspond to propagating FGWs and provide a tight constraint on the ice stiffness. ThusThis study has demonstrated the exceptional capability of, the DAS array in accurately mapping the internal fractures and monitoring the strength of ice shelves. constitutes an exceptional technology for mapping internal fractures and monitoring the strength of ice shelf.By harnessing the unique sensing capabilities of DAS, we were able to capture detailed seismic signals associated with ice cracking and dynamic flexure, providing valuable insights into the behaviour of ice plates. When combined with other remote sensing techniques, such as those employed by (Massom et al., 2018), DAS has the potential to greatly enhance our understanding and monitoring of ice shelf disintegration. The integration of DAS data with complementary remote sensing observations offers a comprehensive approach to studying ice shelf dynamics. This integrated approach provides a powerful tool for assessing the health and vulnerability of ice shelves, as well as tracking their responses to environmental factors and climate change. Combined with other remote sensing observations (Massom et al., 2018), DAS has a grand potential in understanding and monitoring ice shelf disintegration.

Appendix A: Seismic event detection based on YOLO

We convert the record section of DAS waveforms to images and apply a convolutional neural network (CNN) You Only See Once (YOLO, version 5) *to detect the seismic ev*
− time object detection for video files (Redmon & Farhadi, 2018), *which also has been used to detect micro*
− seismic event for DAS record (Stork et al., 2020). *To enhance the SNR, the DAS data is bandpass filtered to* 5
− 50 *Hz and normalized with respect to the maximum amplitude of the entire record section. We assemble* 6
− second data of all channels (51
− 645) *into an image with* 50% *overlap to prevent misdetection. We then down sample the image to* 600 *by* 600 *pixels and keep each image size to about* 980 *KB.*
To train the AI model, we manually inspected the seismic data of the first 12 *hours and labelled* 60 *AGEs,* 122 *LFEs and* 360 *icequakes. We then divide this dataset into tra*

Appendix B: Seismic event location

We locate the seismic events using an absolute location method based on the neighbourhood algorithm (Sam
/LTA method (Stevenson, 1976) ***to pick arrivals. The short and long time***
− windows are set to* 0.05 *s and* 0.25 *s for icequakes, and* 0.5 *s and* 2.5 *s for LFEs, respectively. To make full use of the waveform information the error of th

Appendix C: Dispersion relation of FGW

The dispersion relation (relation of frequency (f) and wavenumber (k)) for FGW can be written as,

$$= \qquad (1).$$

设置了格式: 字体: 加粗
带格式的: 正文, 缩进: 首行缩进: 2 字符
设置了格式: 字体: Cambria Math
设置了格式: 字体: Cambria Math
设置了格式: 字体: Cambria Math
设置了格式: 字体颜色: 自动设置

g is gravity, k is wavenumber, H is the water depth which is 60 meters in this study. D is the bending modulus, which is a function of ice properties, D = E /12(1−), where E is the Young's modulus, v is the Poisson ratio, h is the ice thickness which is 0.5 meters in this study, is the density of water. Q is due to compression forces, Q = Ph/, where is the density of ice. M is due to the added mass of the ice sheet, M = h /. Q and M are much smaller than gravity and flexural terms and can be neglected. The dispersion equation can be rewritten as,

$$= \quad (2).$$

The Young's Modulus can also be determined with compressional wave velocity Vp, E = (1−), assuming v = 0.33, according to the results from Fig. S3, E is 9.12 GPa.

Data availability

All raw data can be provided by the corresponding authors upon request.

AAuthor contributions

XZ, SN planned the campaign; RL performed the measurements; JX, XZ, CL, FB and HL analysed the data; JX wrote the manuscript draft; JX, XZ, CL, SN, RC, BC and FB reviewed and edited the manuscript.

Code and data availability

The DAS data is available on https://www.zenodo.org/record/7424310. YOLOv5 can be found https://github.com/ultralytics/yolov5. NA code can be found http://rses.anu.edu.au/~malcolm/na/

Competing interests

The authors declare that they have no conflict of interest.

设置了格式: 字体: (中文) Times New Roman, 10 磅, 非倾斜, 字体颜色: 自动设置

设置了格式: 超链接, 字体: (中文) Times New Roman, 10 磅, 非倾斜, 字体颜色: 自动设置

设置了格式: 字体: (中文) Times New Roman, 10 磅, 非倾斜, 字体颜色: 自动设置

设置了格式: 字体: (中文) Times New Roman, 10 磅, 非倾斜, 字体颜色: 自动设置

带格式的: 正文

域代码已更改

Acknowledgements

The authors thank Baoshan Wang, Rui Zou, Yahong Wang for their help on the experiment setup and data requisition. We thank Herb Wang and Daoyuan Sun for their professional suggestions. The authors thank two anonymous reviewers and editors for their constructive comments.

Financial support

This work was supported by the National Natural Science Foundation of China with grant number 42274076.

References

Aster, R. C. and Winberry, J. P.: Glacial seismology, Rep. Prog. Phys., 80, 126801, https://doi.org/10.1088/1361-6633/aa8473, 2017.

Booth, A. D., Christoffersen, P., Schoonman, C., Clarke, A., Hubbard, B., Law, R., Doyle, S. H., Chudley, T. R., and Chalari, A.: Distributed Acoustic Sensing of Seismic Properties in a Borehole Drilled on a Fast-Flowing Greenlandic Outlet Glacier, Geophysical Research Letters, 47, e2020GL088148, https://doi.org/10.1029/2020GL088148, 2020.

Brisbourne, A. M., Kendall, M., Kufner, S.-K., Hudson, T. S., and Smith, A. M.: Downhole distributed acoustic seismic profiling at Skytrain Ice Rise, West Antarctica, The Cryosphere, 15, 3443–3458, https://doi.org/10.5194/tc-15-3443-2021, 2021.

Castongia, E., Wang, H. F., Lord, N., Fratta, D., Mondanos, M., and Chalari, A.: An Experimental Investigation of Distributed Acoustic Sensing (DAS) on Lake Ice, JEEG, 22, 167–176, https://doi.org/10.2113/JEEG22.2.167, 2017.

Chen, Z., Bromirski, P. D., Gerstoft, P., Stephen, R. A., Wiens, D. A., Aster, R. C., and Nyblade, A. A.: Ocean-excited plate waves in the Ross and Pine Island Glacier ice shelves, Journal of Glaciology, 64, 730–744, https://doi.org/10.1017/jog.2018.66, 2018.

Chen, Z., Bromirski, P. D., Gerstoft, P., Stephen, R. A., Lee, W. S., Yun, S., Olinger, S. D., Aster, R. C., Wiens, D. A., and Nyblade, A. A.: Ross Ice Shelf Icequakes Associated With Ocean Gravity Wave Activity, Geophysical Research Letters, 46, 8893–8902, https://doi.org/10.1029/2019GL084123, 2019.

Collins III, C. O., Rogers, W. E., Marchenko, A., and Babanin, A. V.: In situ measurements of an energetic wave event in the Arctic marginal ice zone, Geophysical Research Letters, 42, 1863–1870, https://doi.org/10.1002/2015GL063063, 2015.

Dobretsov, N. L., Ruzhich, V. V., Psakhie, S. G., Chernykh, E. N., Shilko, E. V., Levina, E. A., and Ponomareva, E. I.: Advance in earthquake prediction by physical simulation on the baikal ice cover, Phys Mesomech, 16, 52–61, https://doi.org/10.1134/S1029959913010062, 2013.

Ekström, G., Nettles, M., and Abers, G. A.: Glacial Earthquakes, Science, 302, 622–624, https://doi.org/10.1126/science.1088057, 2003.

Ewing, M., Crary, A. P., and Thorne, A. M., Jr.: Propagation of Elastic Waves in Ice. Part I, Physics, 5, 165–168, https://doi.org/10.1063/1.1745245, 2004.

Fichtner, A., Klaasen, S., Thrastarson, S., Çubuk-Sabuncu, Y., Paitz, P., and Jónsdóttir, K.: Fiber-Optic Observation of Volcanic Tremor through Floating Ice Sheet Resonance, The Seismic Record, 2, 148–155, https://doi.org/10.1785/0320220010, 2022.

Gold, L. W.: On the elasticity of ice plates, Can. J. Civ. Eng., 15, 1080–1084, https://doi.org/10.1139/l88-140, 1988.

Goto, K., H, H., and Y, W.: A study on ice faulting and icequake activity in the lake Suwa, (3) icequake activity and thermal stresses in ice plate, The science reports of the Tohoku University. Fifth series, Tohoku Geophysical Journal, 1980.

de Graaf, K. L., Brandner, P. A., and Penesis, I.: The pressure field generated by a seismic airgun, Experimental Thermal and Fluid Science, 55, 239–249, https://doi.org/10.1016/j.expthermflusci.2014.02.025, 2014.

Helmstetter, A., Nicolas, B., Comon, P., and Gay, M.: Basal icequakes recorded beneath an Alpine glacier (Glacier d'Argentière, Mont Blanc, France): Evidence for stick-slip motion?, Journal of Geophysical Research: Earth Surface, 120, 379–401, https://doi.org/10.1002/2014JF003288, 2015.

Hudson, T. S., Baird, A. F., Kendall, J. M., Kufner, S. K., Brisbourne, A. M., Smith, A. M., Butcher, A., Chalari, A., and Clarke, A.: Distributed Acoustic Sensing (DAS) for Natural Microseismicity Studies: A Case Study From Antarctica, Journal of Geophysical Research: Solid Earth, 126, e2020JB021493, https://doi.org/10.1029/2020JB021493, 2021.

Kavanaugh, J., Schultz, R., Andriashek, L. D., van der Baan, M., Ghofrani, H., Atkinson, G., and Utting, D. J.: A New Year's Day icebreaker: icequakes on lakes in Alberta, Canada, Canadian Journal of Earth Sciences, 56, 183–200, https://doi.org/10.1139/cjes-2018-0196, 2018.

Köhler, A., Maupin, V., Nuth, C., and Pelt, W. van: Characterization of seasonal glacial seismicity from a single-station on-ice record at Holtedahlfonna, Svalbard, Annals of Glaciology, 60, 23–36, https://doi.org/10.1017/aog.2019.15, 2019.

Lindsey, N. J., Dawe, T. C., and Ajo-Franklin, J. B.: Illuminating seafloor faults and ocean dynamics with dark fiber distributed acoustic sensing, Science, 366, 1103–1107, https://doi.org/10.1126/science.aay5881, 2019.

Liu, A. K. and Mollo-Christensen, E.: Wave Propagation in a Solid Ice Pack, Journal of Physical Oceanography, 18, 1702–1712, https://doi.org/10.1175/1520-0485(1988)018<1702:WPIASI>2.0.CO;2, 1988.

Lombardi, D., Gorodetskaya, I., Barruol, G., and Camelbeeck, T.: Thermally induced icequakes detected on blue ice areas of the East Antarctic ice sheet, Annals of Glaciology, 60, 45–56, https://doi.org/10.1017/aog.2019.26, 2019.

Massom, R. A., Scambos, T. A., Bennetts, L. G., Reid, P., Squire, V. A., and Stammerjohn, S. E.: Antarctic ice shelf disintegration triggered by sea ice loss and ocean swell, Nature, 558, 383–389, https://doi.org/10.1038/s41586-018-0212-1, 2018.

Moreau, L., Boué, P., Serripierri, A., Weiss, J., Hollis, D., Pondaven, I., Vial, B., Garambois, S., Larose, É., Helmstetter, A., Stehly, L., Hillers, G., and Gilbert, O.: Sea Ice Thickness and Elastic Properties From the Analysis of Multimodal Guided Wave Propagation Measured With a Passive Seismic Array, Journal of Geophysical Research: Oceans, 125, e2019JC015709, https://doi.org/10.1029/2019JC015709, 2020.

Ning, I. L. C. and Sava, P.: High-resolution multi-component distributed acoustic sensing, Geophysical Prospecting, 66, 1111–1122, https://doi.org/10.1111/1365-2478.12634, 2018.

Northwood, T. D.: Sonic determination of the elastic properties of ice, Can. J. Res., 25a, 88–95, https://doi.org/10.1139/cjr47a-011, 1947.

Nziengui-Bâ, D., Coutant, O., Moreau, L., and Boué, P.: Measuring the thickness and Young's modulus of the ice pack with DAS, a test case on a frozen mountain lake, Geophysical Journal International, ggac504, https://doi.org/10.1093/gji/ggac504, 2022.

Olinger, S. D., Lipovsky, B. P., Wiens, D. A., Aster, R. C., Bromirski, P. D., Chen, Z., Gerstoft, P., Nyblade, A. A., and Stephen, R. A.: Tidal and Thermal Stresses Drive Seismicity Along a Major Ross Ice Shelf Rift, Geophysical Research Letters, 46, 6644–6652, https://doi.org/10.1029/2019GL082842, 2019.

Park, C. B., Miller, R. D., and Xia, J.: Multimodal analysis of high frequency surface waves, in: Proceedings of the symposium on the application of geophysics to engineering and environmental problems, 00000, 115–121, 1999.

Parker, L. M., Thurber, C. H., Zeng, X., Li, P., Lord, N. E., Fratta, D., Wang, H. F., Robertson, M. C., Thomas, A. M., Karplus, M. S., Nayak, A., and Feigl, K. L.: Active-Source Seismic Tomography at the Brady Geothermal Field, Nevada, with Dense Nodal and Fiber-Optic Seismic Arrays, Seismological Research Letters, 89, 1629–1640, https://doi.org/10.1785/0220180085, 2018.

Petrovic, J. J.: Review Mechanical properties of ice and snow, Journal of Materials Science, 38, 1–6, https://doi.org/10.1023/A:1021134128038, 2003.

Podolskiy, E. A. and Walter, F.: Cryoseismology, Reviews of Geophysics, 54, 708–758, https://doi.org/10.1002/2016RG000526, 2016.

Redmon, J. and Farhadi, A.: YOLOv3: An incremental improvement, ArXiv, abs/184.02767, 2018.

Romeyn, R., Hanssen, A., Ruud, B. O., Stemland, H. M., and Johansen, T. A.: Passive seismic recording of cryoseisms in Adventdalen, Svalbard, The Cryosphere, 15, 283–302, https://doi.org/10.5194/tc-15-283-2021, 2021.

Röösli, C., Walter, F., Husen, S., Andrews, L. C., Lüthi, M. P., Catania, G. A., and Kissling, E.: Sustained seismic tremors and icequakes detected in the ablation zone of the Greenland ice sheet, Journal of Glaciology, 60, 563–575, https://doi.org/10.3189/2014JoG13J210, 2014.

Ross, Z. E., Meier, M.-A., and Hauksson, E.: P Wave Arrival Picking and First-Motion Polarity Determination With Deep Learning, Journal of Geophysical Research: Solid Earth, 123, 5120–5129, https://doi.org/10.1029/2017JB015251, 2018.

Ruzhich, V. V., Psakhie, S. G., Chernykh, E. N., Bornyakov, S. A., and Granin, N. G.: Deformation and seismic effects in the ice cover of Lake Baikal, Russian Geology and Geophysics, 50, 214–221, https://doi.org/10.1016/j.rgg.2008.08.005, 2009.

Rydelek, P. A. and Sacks, I. S.: Testing the completeness of earthquake catalogues and the hypothesis of self-similarity, Nature, 337, 251–253, https://doi.org/10.1038/337251a0, 1989.

Sambridge, M.: Geophysical inversion with a neighbourhood algorithm—I. Searching a parameter space, Geophysical Journal International, 138, 479–494, https://doi.org/10.1046/j.1365-246X.1999.00876.x, 1999.

Selker, J., van de Giesen, N., Westhoff, M., Luxemburg, W., and Parlange, M. B.: Fiber optics opens window on stream dynamics, Geophysical Research Letters, 33, https://doi.org/10.1029/2006GL027979, 2006.

Sergeant, A., Mangeney, A., Yastrebov, V. A., Walter, F., Montagner, J.-P., Castelnau, O., Stutzmann, E., Bonnet, P., Ralaiarisoa, V. J.-L., Bevan, S., and Luckman, A.: Monitoring Greenland ice sheet buoyancy-driven calving discharge using glacial earthquakes, Annals of Glaciology, 60, 75–95, https://doi.org/10.1017/aog.2019.7, 2019.

Sergienko, O. V.: Behavior of flexural gravity waves on ice shelves: Application to the Ross Ice Shelf, Journal of Geophysical Research: Oceans, 122, 6147–6164, https://doi.org/10.1002/2017JC012947, 2017.

Sinha, N. K.: Elasticity of natural types of polycrystalline ice, Cold Regions Science and Technology, 17, 127–135, https://doi.org/10.1016/S0165-232X(89)80003-5, 1989.

Stevenson, P. R.: Microearthquakes at Flathead Lake, Montana: A study using automatic earthquake processing, The Bulletin of the Seismological Society of America, 66, 61–80, https://doi.org/10.1785/BSSA0660010061, 1976.

Stork, A. L., Baird, A. F., Horne, S. A., Naldrett, G., Lapins, S., Kendall, J.-M., Wookey, J., Verdon, J. P., Clarke, A., and Williams, A.: Application of machine learning to microseismic event detection in distributed acoustic sensing data, GEOPHYSICS, 85, KS149–KS160, https://doi.org/10.1190/geo2019-0774.1, 2020.

Sutherland, G. and Rabault, J.: Observations of wave dispersion and attenuation in landfast ice, Journal of Geophysical Research: Oceans, 121, 1984–1997, https://doi.org/10.1002/2015JC011446, 2016.

Timco, G. W. and Frederking, R. M. W.: Flexural strength and fracture toughness of sea ice, Cold Regions Science and Technology, 8, 35–41, https://doi.org/10.1016/0165-232X(83)90015-0, 1983.

Veitch, S. A. and Nettles, M.: Assessment of glacial-earthquake source parameters, Journal of Glaciology, 63, 867–876, https://doi.org/10.1017/jog.2017.52, 2017.

Walter, F., Dalban Canassy, P., Husen, S., and Clinton, J. F.: Deep icequakes: What happens at the base of Alpine glaciers?, Journal of Geophysical Research: Earth Surface, 118, 1720–1728, https://doi.org/10.1002/jgrf.20124, 2013.

Walter, F., Gräff, D., Lindner, F., Paitz, P., Köpfli, M., Chmiel, M., and Fichtner, A.: Distributed acoustic sensing of microseismic sources and wave propagation in glaciated terrain, Nature Communications, 11, 2436, https://doi.org/10.1038/s41467-020-15824-6, 2020.

Wei, C., Qin, M., Zhang, Y., Zou, R., Wang, L., Guo, X., Liu, X., Wang, Y., and Sun, D.: Airgun Excitation Experiments at Different Placement Depths in the Qilian Mountain of Gansu Province, China, Seismological Research Letters, 89, 974–982, https://doi.org/10.1785/0220170253, 2018.

Wen, T., Garrison, G. R., Francois, R. E., Stein, R. P., and Felton, W. J.: Sound Speed, Reflectivity, and Absorption Measurements in Arctic Ice in 1988, sound speed reflectivity & absorption measurements in arctic ice in, 1991.

West, M. E., Larsen, C. F., Truffer, M., O'Neel, S., and LeBlanc, L.: Glacier microseismicity, Geology, 38, 319–322, https://doi.org/10.1130/G30606.1, 2010.

Williams, R. T. and Robinson, E. S.: Flexural waves in the Ross Ice Shelf, Journal of Geophysical Research: Oceans, 86, 6643–6648, https://doi.org/10.1029/JC086iC07p06643, 1981.

Yang, T. C. and Yates, T. W.: Flexural waves in a floating ice sheet: Modeling and comparison with data, The Journal of the Acoustical Society of America, 97, 971–977, https://doi.org/10.1121/1.412076, 1995.

Zhou, Y., Yue, H., Kong, Q., and Zhou, S.: Hybrid Event Detection and Phase-Picking Algorithm Using Convolutional and Recurrent Neural Networks, Seismological Research Letters, 90, 1079–1087, https://doi.org/10.1785/0220180319, 2019.

Zhu, W. and Beroza, G. C.: PhaseNet: a deep-neural-network-based seismic arrival-time picking method, Geophysical Journal International, 216, 261–273, https://doi.org/10.1093/gji/ggy423, 2019.

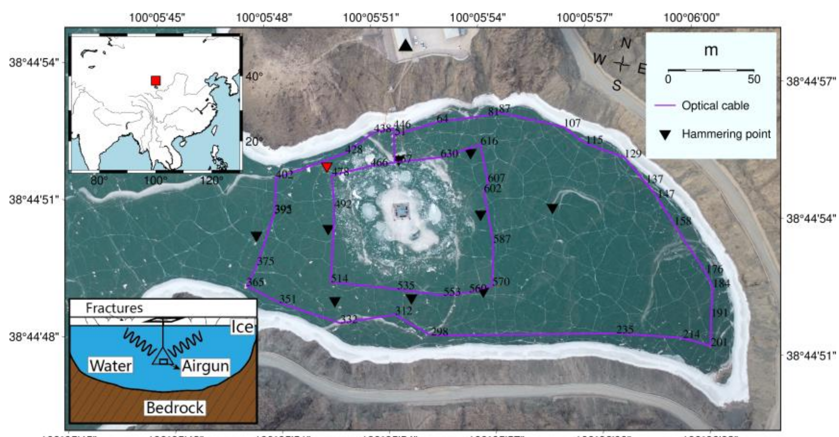

Figure 1: The experimental setting. The instrumented frozen lake is at Xiliushui Reservoir in Gansu Province, China (red rectangle in the inset). The optical fibre is marked with purple lines with channel number between 51-645 with gauge length of 10 m and a sampling rate of 1000 Hz. The airgun floating platform is at the centre of the lake. A reference broadband seismic station is marked with a triangle. Hammering points are marked with inverted triangles. The red triangle shows the one we use to measure the dispersion curve of flexural-gravity wave.

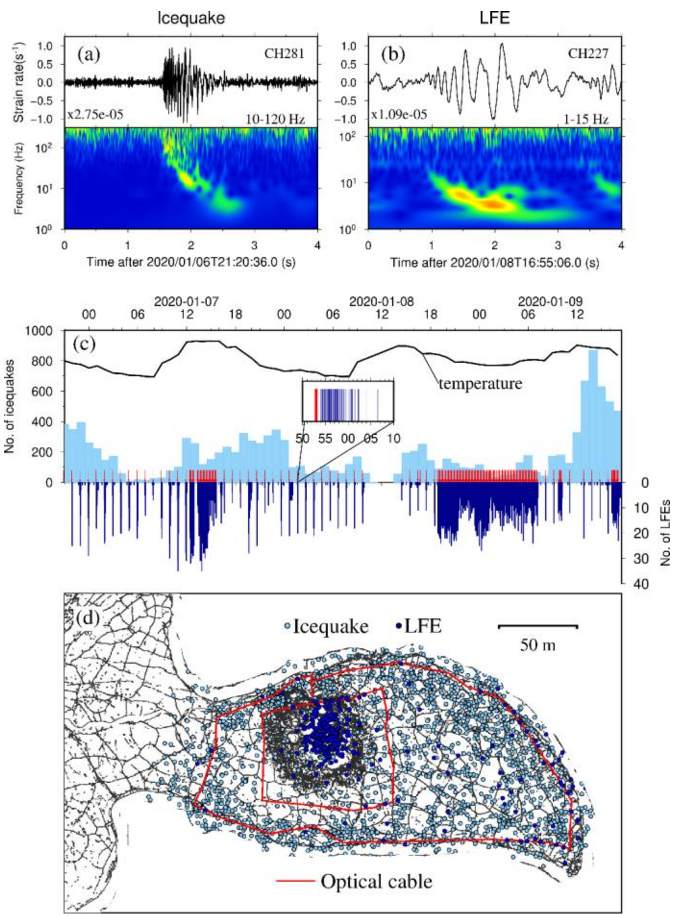

Figure 2: Typical passive signal waveforms, temporal and spatial distributions. (a) Icequake wave recorded by channel 281. The waveform is bandpass filtered in the frequency band of 10-120 Hz. (b) LFE waveform by channel 227. The waveform is bandpass filtered in the frequency band of 1-15 Hz. (c) temporal distributions for icequakes (light blue) per hour and LFEs (dark blue) per minute. The time of AGE is marked with red arrow. The inset picture shows a window of 20 minutes with an AGE (red line) and following LFEs (black lines). The air temperature is denoted with black curve. (d) spatial distribution for icequakes (light blue) and LFEs (dark blue).

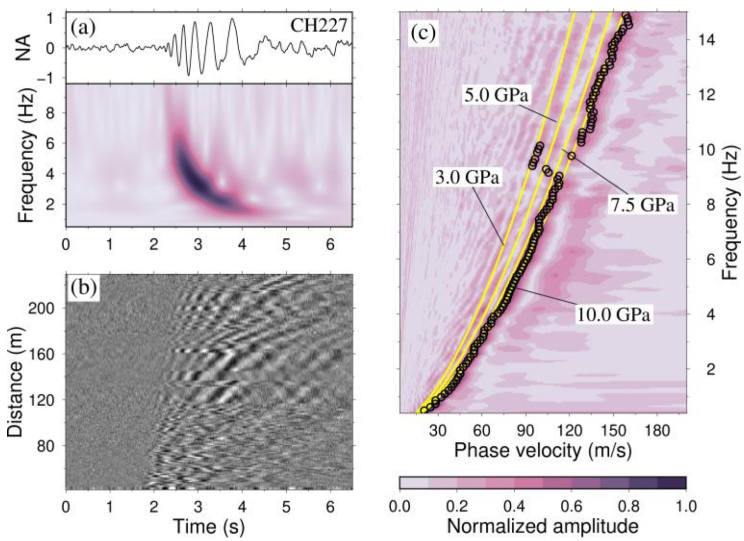

Figure 3: Dispersion analysis of LFEs. (a) Stacked LFE waveform and spectrogram of channel 227. The black curve is the stacked waveform with 272 LFE traces. It is bandpass filtered in the frequency band 1-15 Hz. The color denotes the normalized amplitude. (b) The record section of stacked waveform of all LFE events assuming all LFEs are originated at the AGE platform. (c) The measured phase velocity (circles) and predicted velocities (yellow curves) with different Young's modulus (3-10 GPa). The color means the dispersion spectra of stacked LFE traces in (c).